

Spirals, vortices, and helicity entanglements in dynamical Sauter-Schwinger pair creation

M. M. Majczak, K. Krajewska,* A. Bechler, and J. Z. Kamiński†

*Institute of Theoretical Physics, Faculty of Physics,
University of Warsaw, Pasteura 5, 02-093 Warsaw, Poland*

(Dated: July 14, 2025)

We study helicity correlations of electron-positron pairs created by a homogeneous time-dependent electric field in the Sauter-Schwinger scenario. Our analysis is based on solving the Dirac equation with the Feynman or anti-Feynman boundary conditions, which is equivalent to the scattering matrix approach widely used in high energy physics. Most importantly, both these methods allow to fully account for the helicity (or, more generally, spin) correlations of created particles. The influence of helicity correlations and the carrier-envelope phase of the electric pulse on the properties of topological structures (such as spirals and vortices) in momentum distributions of created particles is investigated. The generation of maximally entangled helicity states is discussed and the possibility of using a short electric pulse as a fast switch between them is indicated.

I. INTRODUCTION

Modern relativistic quantum field theories are based on ideas and methods developed by Dirac [1], Tomonaga [2], Feynman [3, 4], Schwinger [5], and Dyson [6, 7] (see, also, the original papers collected in the book [8]). In particular, Schwinger reformulated achievements of Heisenberg and Euler [9], and Sauter [10] such that it became possible to account for the radiative corrections in quantum electrodynamics (QED). In consequence, this led to the complex effective Lagrangian, the imaginary part of which determines the probability density rates for the electron-positron pair creation by constant electromagnetic fields. Equally fundamental for the further development of the relativistic field theories in general and QED in particular, were the investigations of Feynman. They allowed to reinterpret the concept of anti-particles such that positrons are in fact electrons, but moving backward in time. These and related achievements can be found in the well-known Schweber's textbook [11], or in the review articles [12–14].

The aim of this paper is to investigate the Sauter-Schwinger electron-positron pair creation by time-dependent electric field pulses. A frequently used method for analyzing this process is the approach based on the Dirac-Heisenberg-Wigner (DHW) function [15] (see, also Ref. [16] for the nonrelativistic version). It is based on the second quantization formalism and leads to the so-called system of Quantum Kinetic Equations (QKE) for momentum and spin distributions of created electrons [17–26], but not for the correlated electron and positron spin distributions (see also the Computational Quantum Field Theory [27] which is, however, beyond the scope of our presentation). It has been shown in Ref. [28] that, for spatially homogeneous electric fields, the DHW and QKE approaches follow directly from the Dirac equation pro-

vided that the proper boundary conditions are imposed on the solutions of this wave equation. Additionally, in order to get the same initial conditions (as only in this case both approaches lead to exactly same predictions), the solutions of the Dirac equation in the remote past for positrons have to be normalized to one. This extra requirement may raise some doubts, since in the Sauter-Schwinger process there are no real particles in the past. Both electrons and positrons appear in the form of virtual excitations of the quantum vacuum and, as such, do not have to be on the mass shell. To solve this dilemma, in Ref. [29] an alternative approach to the dynamical Sauter-Schwinger process, based on the scattering matrix and reduction formulas, has been presented. As it results from the formalism developed there, the initial state is uniquely fixed by imposing strictly defined boundary conditions on the solutions of the Dirac equation. Namely, it must be the Feynman boundary condition when we determine the spin and momentum distributions of electrons in the far future for fixed spin and momentum of the created positron. Conversely, if we fix the spin and momentum of the created electron, then the spin-momentum distributions of the positrons are determined by such solutions of the Dirac equation that satisfy the anti-Feynman boundary conditions. Both these boundary conditions are going to be discussed in detail below. The initial condition defined in this way depends on the spins of the created particles and is not normalized to one. As it follows from the analysis presented in Ref. [29], only for electric field strengths much smaller than the Schwinger critical value \mathcal{E}_S this normalization is very close to one. Therefore, one concludes that for the electric field strength such that $|\mathcal{E}(t)| \ll \mathcal{E}_S$ both approaches give nearly identical results for the momentum distributions summed over the spins of created particles. Note that the above boundary conditions, that strictly follow from the scattering matrix and reduction formulas, make difference between the relativistic quantum field theories and the condensed matter physics. For the latter, electrons do exist in the remote past in the form of the occupied valence bands (or the so-called Dirac sea), therefore their states can be

* Katarzyna.Krajewska@fuw.edu.pl

† Jerzy.Kaminski@fuw.edu.pl

normalized.

The approach based on the scattering matrix and reduction formulas provides the complete information about the complex probability amplitudes for the pair creation process and about the electron and positron spin correlations, in contrast to the DHW and QKE formalisms. This opens up new research perspectives for the strong-field QED in general (see, e.g., [30–32]) and for the creation of electron-positron pairs by classical electric fields in particular. For instance, problems related to the topological properties of helicity-momentum distributions and quantum entanglement of helicity states can be investigated now, as discussed below.

The plan of this paper is the following. In Sec. II we show how the fully correlated electron-positron spin-resolved momentum distributions follow directly from the Dirac equation. This leads us to the exact same probability amplitudes and helicity-momentum distributions that can be derived by applying the more sophisticated approach based on the scattering matrix and reduction formulas, presented in Ref. [29]. The Feynman and anti-Feynman boundary conditions are introduced in Sec. III, where we also demonstrate how the corresponding probability amplitudes can be evaluated by applying the transfer matrix discussed in Sec. II C. Topological structures in momentum distributions, such as spirals and vortex lines, are discussed in Sec. IV. We show there that although the existence of spiral distributions are not crucially influenced by the helicity correlations of the created pair, the occurrence of vortex lines significantly depends on these correlations and on the properties of the applied electric field. In particular, the change of the phase of the electric field strongly affects the shape of the vortex lines and, depending on the helicity degrees of freedom, can lead to their annihilation or flattening. Sec. V is devoted to the analysis of quantum entanglement of helicity states of created pairs. We show that the generated entangled state can be effectively controlled by the applied electric field. In particular, a suitable change of electric pulses can be used as a fast switch between orthogonal entangled helicity states. Finally, our conclusions are presented in Sec. VI.

In numerical analysis, we use the relativistic units in which $\hbar = c = m_e = |e| = 1$ and $e = -|e|$, where m_e and e are the electron rest mass and charge. The Schwinger value for the electric field strength, \mathcal{E}_S , is defined such that $m_e c^2 = |e| \mathcal{E}_S \lambda_C$, where $\lambda_C = \hbar/m_e c$ is the reduced Compton wavelength. Additionally, the Compton time is defined as $t_C = \hbar/m_e c^2$. For the γ matrices we apply the Dirac representation, use the Feynman's notation $\not{a} = a_\mu \gamma^\mu$, and the metric $(+, -, -, -)$. In analytical formulas we put $\hbar = 1$ but keep explicitly m_e , e , and c .

II. SOLUTIONS OF THE DIRAC EQUATION

We start by introducing the basic definitions and notation that will be used throughout the paper. Specifically,

we define normalized free bispinors,

$$u_{\mathbf{p},\lambda}^{(+)} = \sqrt{\frac{p^0 + m_e c}{2p^0}} \begin{pmatrix} \chi_\lambda \\ \frac{\boldsymbol{\sigma} \cdot \mathbf{p}}{p^0 + m_e c} \chi_\lambda \end{pmatrix}, \quad (1)$$

$$u_{-\mathbf{p},\lambda}^{(-)} = \sqrt{\frac{p^0 + m_e c}{2p^0}} \begin{pmatrix} \frac{-\boldsymbol{\sigma} \cdot \mathbf{p}}{p^0 + m_e c} \chi_\lambda \\ \chi_\lambda \end{pmatrix}, \quad (2)$$

where $p^0 = \sqrt{\mathbf{p}^2 + (m_e c)^2}$, $\lambda = \pm$, and

$$\chi_+ = \begin{pmatrix} \cos \frac{\theta_s}{2} e^{-i\varphi_s/2} \\ \sin \frac{\theta_s}{2} e^{i\varphi_s/2} \end{pmatrix}, \quad \chi_- = \begin{pmatrix} -\sin \frac{\theta_s}{2} e^{-i\varphi_s/2} \\ \cos \frac{\theta_s}{2} e^{i\varphi_s/2} \end{pmatrix}. \quad (3)$$

If $\mathbf{n} = (\sin \theta_s \cos \varphi_s, \sin \theta_s \sin \varphi_s, \cos \theta_s)$ is the axis of spin quantization, then we have

$$(\boldsymbol{\sigma} \cdot \mathbf{n}) \chi_\pm = \pm \chi_\pm. \quad (4)$$

In particular, if θ_s and φ_s are the polar and azimuthal angles of \mathbf{p} , respectively (or, in other words, if $\mathbf{p} = |\mathbf{p}| \mathbf{n}$), we recover the helicity states for electrons [Eq. (1)] and positrons [Eq. (2)]. Such normalized bispinors are solutions of the system of algebraic equations,

$$(\not{p} - \beta m_e c) u_{\mathbf{p},\lambda}^{(\beta)} = 0, \quad \beta = \pm. \quad (5)$$

The four bispinors [Eqs. (1) and (2)] form the orthonormal basis, as they fulfill the normalization and completeness conditions,

$$[u_{\beta\mathbf{p},\lambda}^{(\beta)}]^\dagger u_{\beta'\mathbf{p},\lambda'}^{(\beta')} = \delta_{\beta\beta'} \delta_{\lambda\lambda'} \quad (6)$$

$$\sum_{\beta,\lambda=\pm} u_{\beta\mathbf{p},\lambda}^{(\beta)} [u_{\beta\mathbf{p},\lambda}^{(\beta)}]^\dagger = \mathbb{I}, \quad (7)$$

where \mathbb{I} is the 4×4 identity matrix. Moreover, the bispinors with $\beta = +$ describe free electrons, whereas those for $\beta = -$ correspond to positrons.

For our further purposes, we order these bispinors as follows,

$$w_{\mathbf{p},1} = u_{\mathbf{p},+}^{(+)}, \quad w_{\mathbf{p},2} = u_{\mathbf{p},-}^{(+)}, \quad w_{\mathbf{p},3} = u_{-\mathbf{p},+}^{(-)}, \quad w_{\mathbf{p},4} = u_{-\mathbf{p},-}^{(-)}. \quad (8)$$

This means that we establish the equivalence,

$$w_{\mathbf{p},j} = u_{\beta\mathbf{p},\lambda}^{(\beta)}, \quad j = 1, \dots, 4, \quad (\beta, \lambda) = (\pm, \pm), \quad (9)$$

with the unique relation $j \leftrightarrow (\beta, \lambda)$. Next, we introduce the unitary matrix,

$$B_{\mathbf{p}} = (w_{\mathbf{p},1}, w_{\mathbf{p},2}, w_{\mathbf{p},3}, w_{\mathbf{p},4}), \quad (10)$$

which relates the bispinor basis $w_{\mathbf{p},j}$ with the canonical one e_j ($j = 1, 2, 3, 4$),

$$w_{\mathbf{p},j} = B_{\mathbf{p}} \cdot e_j, \quad B_{\mathbf{p}}^\dagger B_{\mathbf{p}} = \mathbb{I}. \quad (11)$$

The elements of the latter are columns with zeros everywhere except for the j -th row, whose value is 1. This basis transformation will turn out particularly useful when the time-evolution matrix for the Dirac equation will be constructed.

A. Dirac equation in a time-dependent electric field

Our aim is to analyze solutions of the Dirac equation in the time-dependent electric field $\mathcal{E}(t)$,

$$i\partial_t\psi(\mathbf{x}, t) = \gamma^0 [c\boldsymbol{\gamma} \cdot (-i\nabla - e\mathbf{A}(t)) + m_e c^2] \psi(\mathbf{x}, t), \quad (12)$$

where the corresponding vector potential is defined as

$$\mathbf{A}(t) = \int_t^\infty d\tau \mathcal{E}(\tau). \quad (13)$$

In this case, we seek solutions of Eq. (12) in the form of plane waves,

$$\psi(\mathbf{x}, t) = e^{i\mathbf{p} \cdot \mathbf{x}} \psi_{\mathbf{p}}(t). \quad (14)$$

This leads to the system of four complex ordinary differential equations,

$$i\dot{\psi}_{\mathbf{p}}(t) = H_D(\mathbf{p}, t) \psi_{\mathbf{p}}(t), \quad (15)$$

where the dot over ψ means the time-derivative and the time-dependent Hermitian matrix $H_D(\mathbf{p}, t)$ is equal to

$$H_D(\mathbf{p}, t) = \gamma^0 [c\boldsymbol{\gamma} \cdot (\mathbf{p} - e\mathbf{A}(t)) + m_e c^2]. \quad (16)$$

In general, we assume that

$$\lim_{t \rightarrow \pm\infty} e\mathbf{A}(t) = \mathbf{p}_{\pm}. \quad (17)$$

In practice, however, the above limits mean that there are times $t_i < t_f$ such that $e\mathbf{A}(t) = \mathbf{p}_-$ for $t < t_i$ and $e\mathbf{A}(t) = \mathbf{p}_+$ for $t > t_f$, which is equivalent to saying that for $t < t_i$ and $t > t_f$ the electric field vanishes, $\mathcal{E}(t) = 0$. Hence, we can define the asymptotic free-states,

$$\psi_{\mathbf{p}, \lambda}^{(\beta)}(\mathbf{x}, t) = \exp[-i\beta E_{\mathbf{p}-\mathbf{p}_-}(t - t_i) + i\mathbf{p} \cdot \mathbf{x}] u_{\beta(\mathbf{p}-\mathbf{p}_-), \lambda}^{(\beta)}, \quad (18)$$

for $t \leq t_i$ and

$$\psi_{\mathbf{p}, \lambda}^{(\beta)}(\mathbf{x}, t) = \exp[-i\beta E_{\mathbf{p}-\mathbf{p}_+}(t - t_f) + i\mathbf{p} \cdot \mathbf{x}] u_{\beta(\mathbf{p}-\mathbf{p}_+), \lambda}^{(\beta)}, \quad (19)$$

for $t \geq t_f$, where $E_{\mathbf{p}} = c\sqrt{\mathbf{p}^2 + (m_e c)^2}$. For $\beta = +$ they correspond to electrons of canonical momentum \mathbf{p} and polarizations $\lambda = \pm$, for $\beta = -$ they describe positrons of canonical momentum $-\mathbf{p}$ and polarizations $\lambda = \pm$, whereas $\mathbf{p} - \mathbf{p}_{\pm}$ relate to the kinetic momenta. In the theoretical discussion presented below the name 'momentum' always refers to the canonical momentum. In the numerical analysis, however, we will choose electric field pulses such that $\mathbf{p}_{\pm} = \mathbf{0}$. Hence, the canonical and kinetic momenta are asymptotically identical.

B. Evolution matrix

In order to find a general solution of Eq. (15) we proceed in the standard way. Namely, we introduce the unitary evolution matrix $U_D(\mathbf{p}, t, t')$ that fulfills the differential equation,

$$i\frac{d}{dt}U_D(\mathbf{p}, t, t') = H_D(\mathbf{p}, t)U_D(\mathbf{p}, t, t'), \quad (20)$$

with the initial condition $U_D(\mathbf{p}, t', t') = \mathbb{I}$. Knowing the evolution matrix, one can propagate in time any initial state $\psi_{\mathbf{p}}(t_i)$,

$$\psi_{\mathbf{p}}(t) = U_D(\mathbf{p}, t, t_i) \psi_{\mathbf{p}}(t_i), \quad (21)$$

with the conservation of normalization, $[\psi_{\mathbf{p}}(t)]^\dagger \psi_{\mathbf{p}}(t) = [\psi_{\mathbf{p}}(t_i)]^\dagger \psi_{\mathbf{p}}(t_i)$.

Next, in order to get a more clear physical interpretation of elements of the evolution matrix $U_D(\mathbf{p}, t_f, t_i)$, we introduce another matrix,

$$U_{\mathbf{p}}(t_f, t_i) = B_{\mathbf{p}-\mathbf{p}_+}^\dagger U_D(\mathbf{p}, t_f, t_i) B_{\mathbf{p}-\mathbf{p}_-}. \quad (22)$$

It is also unitary, as it follows from the properties (11). However, only if $\mathbf{p}_- = \mathbf{p}_+$ it satisfies the initial condition $U_{\mathbf{p}}(t_i, t_i) = \mathbb{I}$. Note that this matrix explicitly depends on asymptotic momenta \mathbf{p}_{\pm} , but in order to simplify the notation we shall disregard this dependence in our further analysis. According to the relations (11) between the canonical basis and solutions of the free Dirac equation, the elements of the matrix $U_{\mathbf{p}}$ in the canonical basis have the form,

$$[U_{\mathbf{p}}(t_f, t_i)]_{jk} = w_{\mathbf{p}-\mathbf{p}_+, j}^\dagger U_D(\mathbf{p}, t_f, t_i) w_{\mathbf{p}-\mathbf{p}_-, k}. \quad (23)$$

This shows that columns of $U_{\mathbf{p}}$ have clear physical interpretation. For instance, the first column with elements $[U_{\mathbf{p}}(t_f, t_i)]_{j1}$, corresponding to the initial electron state $u_{\mathbf{p}-\mathbf{p}_-, +}^{(+)}$ [cf. ordering (9)], contains probability amplitudes at time t_f for electrons of momentum \mathbf{p} and spin polarizations \pm (first and second rows), and for positrons of momentum $-\mathbf{p}$ and spin polarizations \pm (third and fourth rows). In a similar way the second column contains probability amplitude for the initial electron state $u_{\mathbf{p}-\mathbf{p}_-, -}^{(+)}$, whereas third and fourth columns correspond to positron initial states $u_{-(\mathbf{p}-\mathbf{p}_-), +}^{(-)}$ and $u_{-(\mathbf{p}-\mathbf{p}_-), -}^{(-)}$, respectively. In general, if the initial state $\psi_{\mathbf{p}}(t_i)$ has the form

$$\psi_{\mathbf{p}}(t_i) = \sum_{\beta, \lambda=\pm} c_{\mathbf{p}, \lambda}^{(\beta)}(t_i) u_{\beta(\mathbf{p}-\mathbf{p}_-), \lambda}^{(\beta)}, \quad (24)$$

then the final state $\psi_{\mathbf{p}}(t_f)$ is equal to

$$\psi_{\mathbf{p}}(t_f) = \sum_{\beta, \lambda=\pm} c_{\mathbf{p}, \lambda}^{(\beta)}(t_f) u_{\beta(\mathbf{p}-\mathbf{p}_+), \lambda}^{(\beta)}. \quad (25)$$

The corresponding amplitudes are related by

$$\mathbb{C}_{\mathbf{p}}(t_f) = U_{\mathbf{p}}(t_f, t_i) \mathbb{C}_{\mathbf{p}}(t_i), \quad (26)$$

where we have introduced the notation,

$$\mathbb{C}_{\mathbf{p}}(t) = \begin{pmatrix} \mathbb{C}_{\mathbf{p}}^{(+)}(t) \\ \mathbb{C}_{\mathbf{p}}^{(-)}(t) \end{pmatrix}, \quad \mathbb{C}_{\mathbf{p}}^{(\beta)}(t) = \begin{pmatrix} c_{\mathbf{p}, +}^{(\beta)}(t) \\ c_{\mathbf{p}, -}^{(\beta)}(t) \end{pmatrix}, \quad (27)$$

with complex amplitudes $c_{\mathbf{p}, \lambda}^{(\beta)}(t)$ such that

$$\sum_{\beta, \lambda=\pm} |c_{\mathbf{p}, \lambda}^{(\beta)}(t)|^2 = 1, \quad (28)$$

for all times, as the evolution matrix is unitary.

A complementary meaning of the elements of $U_{\mathbf{p}}(t_f, t_i)$ can be gained from the time-evolution of the system. First, we define the propagator $U(\mathbf{x}, t; \mathbf{x}', t')$ which fulfills the equation,

$$[i\partial_t - H_D(-i\nabla, t)]U(\mathbf{x}, t; \mathbf{x}', t') = 0, \quad t \geq t', \quad (29)$$

with the initial condition,

$$U(\mathbf{x}, t'; \mathbf{x}', t') = \delta^{(3)}(\mathbf{x} - \mathbf{x}'). \quad (30)$$

Then, the space-time evolution of any initial state $\psi_i(\mathbf{x}, t)$ is given by the space-integral,

$$\psi(\mathbf{x}, t) = \int d^3x' U(\mathbf{x}, t; \mathbf{x}', t') \psi_i(\mathbf{x}', t'). \quad (31)$$

Hence, the transition amplitude to the final state $\psi_f(\mathbf{x}, t)$ within the time-interval $[t, t']$ is equal to

$$\mathcal{A}_{fi}(t, t') = \int d^3x d^3x' [\psi_f(\mathbf{x}, t)]^\dagger U(\mathbf{x}, t; \mathbf{x}', t') \psi_i(\mathbf{x}', t'). \quad (32)$$

Next, since the interaction depends only on time, therefore

$$\begin{aligned} U(\mathbf{x}, t_f; \mathbf{x}', t_i) &= \int \frac{d^3p}{(2\pi)^3} e^{i\mathbf{p}\cdot\mathbf{x}} U_D(\mathbf{p}, t_f, t_i) e^{-i\mathbf{p}\cdot\mathbf{x}'} \\ &= \int \frac{d^3p}{(2\pi)^3} e^{i\mathbf{p}\cdot\mathbf{x}} B_{\mathbf{p}-\mathbf{p}_+} U_{\mathbf{p}}(t_f, t_i) [B_{\mathbf{p}-\mathbf{p}_-}]^\dagger e^{-i\mathbf{p}\cdot\mathbf{x}'}, \end{aligned} \quad (33)$$

and the transition amplitude between the initial stationary state $\psi_{\mathbf{p}_i, \lambda_i}^{(\beta_i)}(\mathbf{x}', t_i)$ [see, Eq. (18)] and the final one $\psi_{\mathbf{p}_f, \lambda_f}^{(\beta_f)}(\mathbf{x}', t_f)$ [see, Eq. (19)] equals

$$\mathcal{A}_{fi} = (2\pi)^3 \delta^{(3)}(\mathbf{p}_f - \mathbf{p}_i) [U_{\mathbf{p}_i}(t_f, t_i)]_{j_f j_i}, \quad (34)$$

where $j_i \leftrightarrow (\beta_i, \lambda_i)$ and $j_f \leftrightarrow (\beta_f, \lambda_f)$, according to the ordering (9). Note that momenta for particles and anti-particles have opposite space directions.

In the definition (22) we have selected times such that either before t_i or after t_f the electric field vanishes. Our choice is motivated by future applications of the theory developed here in which the time-dependent electric field exists only for a finite time and the pair creation is assisted by the entire electric field pulse. If, however, one is interested in the investigation of the process within the electric field pulse, then the more general form of the evolution matrix $U_{\mathbf{p}}(t_f, t_i)$ could be used,

$$U_{\mathbf{p}}(t, t') = B_{\mathbf{p}-e\mathbf{A}(t)}^\dagger U_D(\mathbf{p}, t, t') B_{\mathbf{p}-e\mathbf{A}(t')}, \quad (35)$$

in which temporal basis of the Dirac bispinors, Eqs. (1) and (2), are applied.

C. Transfer matrix

Since the Feynman's pioneering works [3, 4], physical processes of relativistic quantum field theories are predominantly described in terms of the Feynman diagrams.

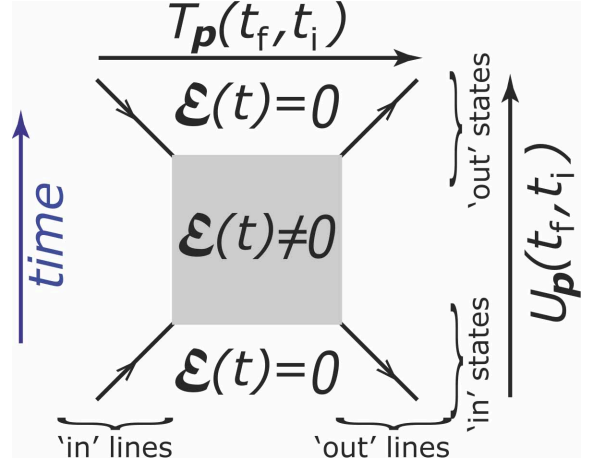


Figure 1. Graphical representation of the time-evolution vs. 'line-evolution' for the Feynman diagram with four external fermion lines.

In QED these diagrams are built off fermion and photon lines, and the external lines that go to infinities represent the real particles. If we choose the time arrow vertically in the 'up-direction', then the fermion lines can be oriented either upwards or downwards: the upward direction describes electrons and the downward one corresponds to positrons. Since for the pair creation process in the final state we have both the electron and positron lines, and in addition we do not have external photon lines, as the time-dependent electric field is treated classically, therefore, also in the initial state we have two lines, one for electrons and another one for positrons. Hence, the initial state for the time-evolution consists of incoming (electron) and outgoing (positron) lines. Similar situation is met for the final state, i.e., outgoing line represents the particle (electron) and the incoming one corresponds to the anti-particle (positron). However, one can look at the Feynman diagram in the horizontal direction and try to relate the incoming lines to the outgoing ones. While in the vertical direction such a process is described by the evolution matrix, in the horizontal direction the transformation of the incoming to the outgoing lines is given by another matrix, which we call below the transfer matrix.

The transfer matrix $T_{\mathbf{p}}(t, t')$ relates the incoming lines to the outgoing ones, i.e.,

$$\begin{pmatrix} \mathbb{C}_{\mathbf{p}}^{(+)}(t) \\ \mathbb{C}_{\mathbf{p}}^{(-)}(t') \end{pmatrix} = T_{\mathbf{p}}(t, t') \begin{pmatrix} \mathbb{C}_{\mathbf{p}}^{(+)}(t') \\ \mathbb{C}_{\mathbf{p}}^{(-)}(t) \end{pmatrix}. \quad (36)$$

It can be derived from the evolution matrix $U_{\mathbf{p}}(t, t')$. To this end let us write

$$U_{\mathbf{p}}(t, t') = \begin{pmatrix} U_{\mathbf{p}}^{(++)}(t, t') & U_{\mathbf{p}}^{(+-)}(t, t') \\ U_{\mathbf{p}}^{(-+)}(t, t') & U_{\mathbf{p}}^{(--)}(t, t') \end{pmatrix} \quad (37)$$

and

$$T_{\mathbf{p}}(t, t') = \begin{pmatrix} T_{\mathbf{p}}^{(++)}(t, t') & T_{\mathbf{p}}^{(+-)}(t, t') \\ T_{\mathbf{p}}^{(-+)}(t, t') & T_{\mathbf{p}}^{(--)}(t, t') \end{pmatrix}, \quad (38)$$

where $U_{\mathbf{p}}^{(\beta\beta')}(t, t')$ and $T_{\mathbf{p}}^{(\beta\beta')}(t, t')$ ($\beta, \beta' = \pm$) are 2×2 matrices. Then, after some algebra, we find,

$$\begin{aligned} T_{\mathbf{p}}^{(++)}(t, t') &= U_{\mathbf{p}}^{(++)}(t, t') \\ &\quad - U_{\mathbf{p}}^{(+-)}(t, t') [U_{\mathbf{p}}^{(--)}(t, t')]^{-1} U_{\mathbf{p}}^{(-+)}(t, t'), \\ T_{\mathbf{p}}^{(+-)}(t, t') &= U_{\mathbf{p}}^{(+-)}(t, t') [U_{\mathbf{p}}^{(--)}(t, t')]^{-1}, \\ T_{\mathbf{p}}^{(-+)}(t, t') &= - [U_{\mathbf{p}}^{(--)}(t, t')]^{-1} U_{\mathbf{p}}^{(-+)}(t, t'), \\ T_{\mathbf{p}}^{(--)}(t, t') &= [U_{\mathbf{p}}^{(--)}(t, t')]^{-1}. \end{aligned} \quad (39)$$

Similarly, the inverse of the transfer matrix relates the outgoing lines to the incoming ones,

$$\begin{pmatrix} \mathbb{C}_{\mathbf{p}}^{(+)}(t') \\ \mathbb{C}_{\mathbf{p}}^{(-)}(t) \end{pmatrix} = [T_{\mathbf{p}}(t, t')]^{-1} \begin{pmatrix} \mathbb{C}_{\mathbf{p}}^{(+)}(t) \\ \mathbb{C}_{\mathbf{p}}^{(-)}(t') \end{pmatrix}. \quad (40)$$

Although the formulas derived above are valid for arbitrary times $t > t'$, we will apply them for $t = t_f$ and $t' = t_i$. A schematic representation of the time-evolution (given by the evolution matrix) and the ‘line-evolution’ (given by the transfer matrix) is shown in Fig. 1. Note that a similar method, but for the transfer and the scattering matrices, has been used in investigations of electron transport phenomena in nanostructures [33, 34].

III. FEYNMAN AND ANTI-FEYNMAN BOUNDARY CONDITIONS

Investigation of dynamics in nonrelativistic quantum mechanics consists in finding solutions of the Schrödinger equation that satisfy the retarded or advanced boundary conditions. However, in relativistic quantum theories, because we deal with free-particle states of negative energy, there exists two extra boundary conditions, which are called the Feynman and anti-Feynman ones [35]. Let us stick further to the physical problem considered in this paper, i.e., to the evolution of solutions of the Dirac equation in the time-dependent electric field that vanishes in the remote past and far future, as described above. We say that the solution $\psi_{\mathbf{F};\mathbf{p},\lambda_0}^{(-)}(\mathbf{x}, t)$ fulfills the Feynman boundary condition if

$$\psi_{\mathbf{F};\mathbf{p},\lambda_0}^{(-)}(\mathbf{x}, t) = \begin{cases} \phi_{\mathbf{p},\lambda_0}^{(-)}(\mathbf{x}, t) + \sum_{\lambda=\pm} \phi_{\mathbf{p},\lambda}^{(+)}(\mathbf{x}, t), & t > t_f, \\ \sum_{\lambda=\pm} \phi_{\mathbf{p},\lambda}^{(-)}(\mathbf{x}, t), & t < t_i, \end{cases} \quad (41)$$

where [see, Eqs. (18) and (19)]

$$\begin{aligned} \phi_{\mathbf{p},\lambda_0}^{(-)}(\mathbf{x}, t) &= e^{iE_{\mathbf{p}-\mathbf{p}_+}(t-t_f)} e^{i\mathbf{p}\cdot\mathbf{x}} u_{-(\mathbf{p}-\mathbf{p}_+),\lambda_0}^{(-)}, \\ \phi_{\mathbf{p},\lambda}^{(+)}(\mathbf{x}, t) &= e^{-iE_{\mathbf{p}-\mathbf{p}_+}(t-t_f)} e^{i\mathbf{p}\cdot\mathbf{x}} c_{\mathbf{p},\lambda}^{(+)}(t_f) u_{\mathbf{p}-\mathbf{p}_+,\lambda}^{(+)}, \\ \phi_{\mathbf{p},\lambda}^{(-)}(\mathbf{x}, t) &= e^{iE_{\mathbf{p}-\mathbf{p}_-}(t-t_i)} e^{i\mathbf{p}\cdot\mathbf{x}} c_{\mathbf{p},\lambda}^{(-)}(t_i) u_{-(\mathbf{p}-\mathbf{p}_-),\lambda}^{(-)}, \end{aligned} \quad (42)$$

and $E_{\mathbf{p}} = \sqrt{(c\mathbf{p})^2 + (m_e c^2)^2}$.

As we see, for the Feynman boundary conditions in the past we have *a priori* an arbitrary combination of only free-particle positron states of momentum $-\mathbf{p}$. On the other hand, in the future we meet again *a priori* an arbitrary superposition of electron states of momentum \mathbf{p} , and the well-defined positron state of momentum $-\mathbf{p}$ and the spin-polarization λ_0 . Arbitrary so far constant complex numbers $c_{\mathbf{p},\lambda}^{(+)}(t_f)$ and $c_{\mathbf{p},\lambda}^{(-)}(t_i)$ depend also on λ_0 , but in order not to complicate the notation we shall disregard this dependence. Next, as the function $\psi_{\mathbf{F};\mathbf{p},\lambda_0}^{(-)}(\mathbf{x}, t)$ is supposed to satisfy the Dirac equation for all times, these constants are determined by the transfer matrix,

$$\begin{pmatrix} c_{\mathbf{p},+}^{(+)}(t_f) \\ c_{\mathbf{p},-}^{(+)}(t_f) \\ c_{\mathbf{p},+}^{(-)}(t_i) \\ c_{\mathbf{p},-}^{(-)}(t_i) \end{pmatrix} = T_{\mathbf{p}}(t_f, t_i) \begin{pmatrix} 0 \\ 0 \\ \delta_{+,\lambda_0} \\ \delta_{-,\lambda_0} \end{pmatrix}, \quad (43)$$

and fulfill the normalization condition,

$$1 + \sum_{\lambda=\pm} |c_{\mathbf{p},\lambda}^{(+)}(t_f)|^2 = \sum_{\lambda=\pm} |c_{\mathbf{p},\lambda}^{(-)}(t_i)|^2. \quad (44)$$

Let us further introduce the real number $N_{\mathbf{p}}^{(-)}(t_i)$ such that

$$[N_{\mathbf{p}}^{(-)}(t_i)]^2 = \sum_{\lambda=\pm} |c_{\mathbf{p},\lambda}^{(-)}(t_i)|^2, \quad (45)$$

and rewrite Eq. (44) in the form

$$\sum_{\lambda=\pm} |\mathcal{A}_{\lambda_0}^{(+)}(\mathbf{p}, \lambda)|^2 = \sum_{\lambda=\pm} P_{\lambda_0}^{(+)}(\mathbf{p}, \lambda) = P_{\lambda_0}^{(-)}(\mathbf{p}), \quad (46)$$

where

$$\mathcal{A}_{\lambda_0}^{(+)}(\mathbf{p}, \lambda) = c_{\mathbf{p},\lambda}^{(+)}(t_f), \quad (47)$$

$$P_{\lambda_0}^{(+)}(\mathbf{p}, \lambda) = |\mathcal{A}_{\lambda_0}^{(+)}(\mathbf{p}, \lambda)|^2, \quad (48)$$

and

$$P_{\lambda_0}^{(-)}(\mathbf{p}) = [N_{\mathbf{p}}^{(-)}(t_i)]^2 - 1. \quad (49)$$

According to the Feynman original analysis [3, 4], also discussed in the textbook [35], $P_{\lambda_0}^{(-)}(\mathbf{p})$ can be interpreted as the momentum distribution of created positrons of momentum $-\mathbf{p}$ and spin polarization λ_0 . Moreover, $P_{\lambda_0}^{(+)}(\mathbf{p}, \lambda)$ is the momentum distribution of created electrons of momentum \mathbf{p} and spin polarization λ , provided that the spin polarization of accompanied positrons is λ_0 . As it does depend on the spin state of positrons, we shall call it the conditional momentum distribution. The same concerns $\mathcal{A}_{\lambda_0}^{(+)}(\mathbf{p}, \lambda)$, which represents the corresponding complex conditional amplitudes for the electron momentum distributions. This interpretation follows directly from the scattering matrix formalism developed in Ref. [29]. Note that since the electric field is

homogeneous in space, the momenta of created electrons and positrons have opposite space-directions.

A similar procedure should exist for the case in which electrons are generated in the well-defined states and the conditional amplitudes and distributions are determined for accompanying positrons. This goal is achieved if the anti-Feynman boundary conditions are applied.

Following [35] we say that the state $\psi_{\mathbf{d};\mathbf{p},\lambda}^{(+)}(\mathbf{x}, t)$ fulfills the anti-Feynman boundary conditions if asymptotically it behaves as

$$\psi_{\mathbf{d};\mathbf{p},\lambda_0}^{(+)}(\mathbf{x}, t) = \begin{cases} \phi_{\mathbf{p},\lambda_0}^{(+)}(\mathbf{x}, t) + \sum_{\lambda=\pm} \phi_{\mathbf{p},\lambda}^{(-)}(\mathbf{x}, t), & t > t_f, \\ \sum_{\lambda=\pm} \phi_{\mathbf{p},\lambda}^{(+)}(\mathbf{x}, t), & t < t_i, \end{cases} \quad (50)$$

where

$$\begin{aligned} \phi_{\mathbf{p},\lambda_0}^{(+)}(\mathbf{x}, t) &= e^{-iE_{\mathbf{p}-\mathbf{p}_+}(t-t_f)} e^{i\mathbf{p}\cdot\mathbf{x}} u_{\mathbf{p}-\mathbf{p}_+, \lambda_0}^{(+)}, \\ \phi_{\mathbf{p},\lambda}^{(-)}(\mathbf{x}, t) &= e^{iE_{\mathbf{p}-\mathbf{p}_+}(t-t_f)} e^{i\mathbf{p}\cdot\mathbf{x}} c_{\mathbf{p},\lambda}^{(-)}(t_f) u_{-(\mathbf{p}-\mathbf{p}_+), \lambda}^{(-)}, \\ \phi_{\mathbf{p},\lambda}^{(+)}(\mathbf{x}, t) &= e^{-iE_{\mathbf{p}-\mathbf{p}_-}(t-t_i)} e^{i\mathbf{p}\cdot\mathbf{x}} c_{\mathbf{p},\lambda}^{(+)}(t_i) u_{\mathbf{p}-\mathbf{p}_-, \lambda}^{(+)} \end{aligned} \quad (51)$$

Similarly to the Feynman boundary conditions, the unknown coefficients are determined by the inverse of the transfer matrix,

$$\begin{pmatrix} c_{\mathbf{p},+}^{(+)}(t_i) \\ c_{\mathbf{p},-}^{(+)}(t_i) \\ c_{\mathbf{p},+}^{(-)}(t_f) \\ c_{\mathbf{p},-}^{(-)}(t_f) \end{pmatrix} = [T_{\mathbf{p}}(t_f, t_i)]^{-1} \begin{pmatrix} \delta_{+, \lambda_0} \\ \delta_{-, \lambda_0} \\ 0 \\ 0 \end{pmatrix}, \quad (52)$$

from which we obtain momentum distributions and corresponding amplitudes for created particles and anti-particles. Namely, if

$$[N_{\mathbf{p}}^{(+)}(t_i)]^2 = \sum_{\lambda=\pm} |c_{\mathbf{p},\lambda}^{(+)}(t_i)|^2, \quad (53)$$

then

$$\sum_{\lambda=\pm} |\mathcal{A}_{\lambda_0}^{(-)}(\mathbf{p}, \lambda)|^2 = \sum_{\lambda=\pm} P_{\lambda_0}^{(-)}(\mathbf{p}, \lambda) = P_{\lambda_0}^{(+)}(\mathbf{p}). \quad (54)$$

Here,

$$P_{\lambda_0}^{(-)}(\mathbf{p}, \lambda) = |\mathcal{A}_{\lambda_0}^{(-)}(\mathbf{p}, \lambda)|^2 \quad (55)$$

and

$$\mathcal{A}_{\lambda_0}^{(-)}(\mathbf{p}, \lambda) = c_{\mathbf{p},\lambda}^{(-)}(t_f) \quad (56)$$

is the amplitude of created positrons of momentum $-\mathbf{p}$ and polarization λ , provided that electrons of momentum \mathbf{p} and polarization λ_0 are generated with the distribution

$$P_{\lambda_0}^{(+)}(\mathbf{p}) = [N_{\mathbf{p}}^{(+)}(t_i)]^2 - 1. \quad (57)$$

The graphical representation of the Feynman and anti-Feynman boundary conditions are shown in Fig. 2, in which the circles identify those lines that have the well-defined momentum and polarization. Note, however, that for anti-particles the momentum is $-\mathbf{p}$. This representation is based on the corresponding drawings from Ref. [35].

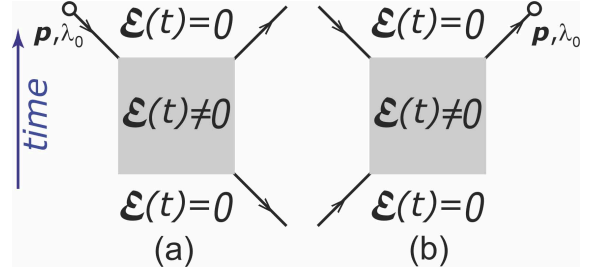


Figure 2. Diagrams representing (a) the state $\psi_{\mathbf{F};\mathbf{p},\lambda_0}^{(-)}(\mathbf{x}, t)$ [cf. Eq. (41)] that satisfies the Feynman boundary conditions and (b) the corresponding state $\psi_{\mathbf{d};\mathbf{p},\lambda_0}^{(+)}(\mathbf{x}, t)$ [cf. Eq. (50)] for the anti-Feynman boundary conditions (cf. Ref. [35], pp. 263 and 265).

IV. SPIRAL AND VORTEX STRUCTURES

Since the seminal research on the spiral structures in photoelectron momentum distributions [36], different aspects of this topic have been investigated. Initially, the existence of spirals was attributed to the creation of quantum vortices. However, the quantum vortex has the well-defined mathematical meaning (investigated already by Dirac [37]; see, also [38–40] and references therein), in contrast to spiral structures, which are only recognized in the visual presentation of the corresponding distributions. Based on this fact it was shown that the momentum spirals in multiphoton ionization (detachment) are not necessarily related to quantum vortices [41]. Complementarily, that quantum vortices are present in distributions that do not exhibit the spiral structures [42–44]. In other words, it was demonstrated that spirals and vortices are different physical concepts in quantum theories. Even more, by changing the form of the laser pulse it is possible to create or annihilate vortex-anti-vortex pairs without affecting the existence of the spiral structures [45]. The point being that the annihilation of the vortex and anti-vortex lines leads to the creation of a nodal surface and *vice versa*, which does preserve the separation between the spiral arms.

The Sauter-Schwinger pair creation by an oscillating electric field and the multiphoton ionization have much in common. This has been shown by applying the spinorial approach [28, 29, 46, 47], equivalent to the quantum two-level systems. However, the shortcoming of this approach is that it does not fully take into account the spin degrees of freedom of both electrons and positrons, and is applicable only for linearly polarized electric fields. We can overcome these problems by using the scattering matrix approach [29] or, equivalently, the formalism presented in this paper. On the other hand, in the ionization of atoms the electron spin does not play an important role and, for this reason, the theoretical analysis mentioned above was carried out using the nonrelativistic Schrödinger theory. Therefore, the question arises: How does taking into account the spin (helicity) correlations of the created elec-

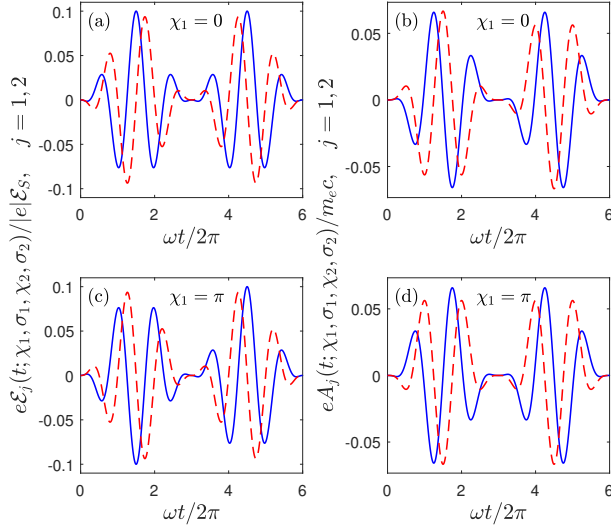


Figure 3. Electric field pulses defined by Eq. (60) [panels (a) and (c)] and the corresponding vector potentials (61) [panels (b) and (d)] for $\mathcal{E}_0 = 0.1\mathcal{E}_S$, $T_p = 2\pi N_{\text{osc}}/\omega$, $N_{\text{osc}} = 3$, $\omega = 1.5m_e c^2$, $\sigma_1 = +1$, $\sigma_2 = -1$, $\chi_2 = 0$, and for two carrier envelope phases of the first pulse: $\chi_1 = 0$ [panels (a) and (b)] and $\chi_1 = \pi$ [panels (c) and (d)]. The solid line represents the x -coordinate (i.e., $j = 1$) of the corresponding vector functions, whereas the dashed line relates to the y -coordinates (i.e., $j = 2$). For these parameters both the electric field and the vector potential vanish asymptotically.

trons and positrons affect the formation of the spiral and vortex structures in the momentum distributions? This is the central focus of this section.

We define an electric field pulse similar to the one used in ionization analysis. In the beginning, let us introduce the envelope function,

$$F(t) = \begin{cases} \sin^2(\pi \frac{t}{T_p}), & \text{for } 0 \leq t \leq T_p, \\ 0, & \text{otherwise,} \end{cases} \quad (58)$$

that acquires nonvanishing values for positive times not longer than T_p . This allows us to define the circularly polarized electric field pulse,

$$\mathcal{E}_0(t; \chi, \sigma) = \mathcal{E}_0 F(t) [\cos(\omega t + \chi) \mathbf{e}_x + \sigma \sin(\omega t + \chi) \mathbf{e}_y], \quad (59)$$

where \mathcal{E}_0 is the electric field amplitude, ω is the frequency of its oscillations, χ is the carrier envelope phase, and $\sigma = \pm 1$ labels the helicity of the electric pulse polarization. Finally, we define the train of two electric pulses,

$$\mathcal{E}(t; \chi_1, \sigma_1, \chi_2, \sigma_2) = \mathcal{E}_0(t; \chi_1, \sigma_1) + \mathcal{E}_0(t - T_p; \chi_2, \sigma_2), \quad (60)$$

and the corresponding vector potential that vanishes in the far future,

$$\mathbf{A}(t; \chi_1, \sigma_1, \chi_2, \sigma_2) = \int_t^\infty d\tau \mathcal{E}(\tau; \chi_1, \sigma_1, \chi_2, \sigma_2). \quad (61)$$

Furthermore, we will assume that each pulse contains N_{osc} cycles; hence, $T_p = 2\pi N_{\text{osc}}/\omega$. Two examples of

such pulses for $N_{\text{osc}} = 3$ and $\mathcal{E}_0 = 0.1\mathcal{E}_S$ are presented in Fig. 3, for different values of the carrier-envelope phase χ_1 . Note that, independently of the field configuration, for $N_{\text{osc}} \geq 2$ both the electric field [Eqs. (59) and (60)] and the vector potential [Eq. (61)] vanish in the far past and future.

The theoretical analysis of determining complex probability amplitudes $\mathcal{A}_{\lambda_0}^{(\beta)}(\mathbf{p}, \lambda)$ presented above concerned the situation when the spin quantization axis of the created particles is fixed, for instance along the z -axis. However, by choosing their linear combinations, we can calculate amplitudes for which the electron and positron spin polarizations are different and arbitrarily directed in space. In our further analysis we will assume that these axes are determined by the electron and positron momenta, which means that we will analyze the amplitudes describing the helicity correlations of created particles. The reason for this choice of spin degrees of freedom is that the helicity operator commutes with the free particle Dirac Hamiltonian (see, e.g., [29, 35] and references therein). This means that the energy and helicity of the electron or positron can be measured simultaneously. Therefore, in the further discussion, the quantities λ and λ_0 appearing in the amplitudes $\mathcal{A}_{\lambda_0}^{(\beta)}(\mathbf{p}, \lambda)$ always denote the helicities of the particles. Additionally, since the momenta of the created electrons and positrons are opposite, without loss of generality only the analysis of electron momentum distributions will be presented, which implies the choice of $\beta = +$. This means that λ and λ_0 are the helicities of created electrons and positrons, respectively.

A. Momentum distributions in the (p_x, p_y) -plane

First, we discuss the electron momentum distributions in the (p_x, p_y) -plane, i.e. for momenta $\mathbf{p} = p_x \mathbf{e}_x + p_y \mathbf{e}_y = p_r (\cos \varphi \mathbf{e}_x + \sin \varphi \mathbf{e}_y)$. In Figs. 4(a) and 4(c) we present the moduli of the amplitudes $\mathcal{A}_-^{(+)}(\mathbf{p}, -)$ for parameters of the electric field pulses defined in the caption to Fig. 3, for $\chi_1 = 0$ and $\chi_1 = \pi$, respectively. Note that for the visual purpose these moduli are raised to the power $\nu = 1/4$ and two copies of them are shown in each panel.

A careful analysis of the presented distributions reveals important differences for $\chi_1 = 0$ and π . In Fig. 4(c) (for $\chi_1 = \pi$) we observe continuous lines of a practically zero amplitude. For the considered electric field pulse these lines are open, i.e., they start and end at the boundaries of the region, even though for longer pulses one can also find closed lines. On the other hand, in Fig. 4(a) (for $\chi_1 = 0$) there are lines of small values of the probability amplitude which end abruptly. To explain this difference it is necessary to discuss the distribution of the phase of the amplitude (the meaning of the extra phase $\phi(\mathbf{p})$ is discussed below)

$$\Phi_{\lambda_0}^{(\beta)}(\mathbf{p}, \lambda) = \arg[e^{i\phi(\mathbf{p})} \mathcal{A}_{\lambda_0}^{(\beta)}(\mathbf{p}, \lambda)], \quad (62)$$

presented in Figs. 4(b) (for $\chi_1 = 0$) and 4(d) (for $\chi_1 = \pi$).

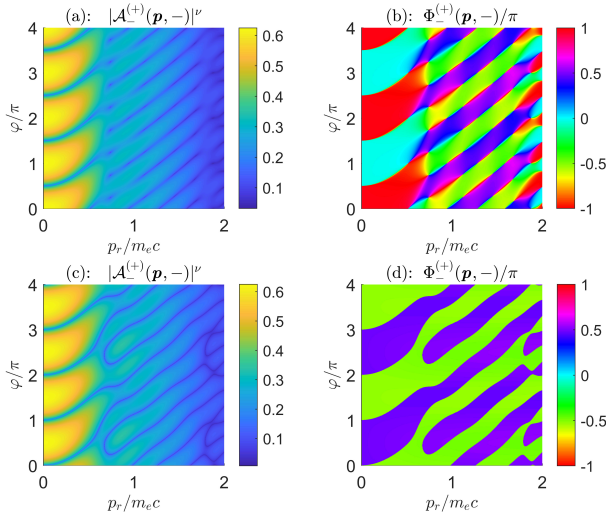


Figure 4. Probability amplitudes $\mathcal{A}^+(\mathbf{p}, -)$ for the electric pulses defined in the caption of Fig. 3 for $p_z = 0$ and for the positron and electron helicities -1 . Panel (a) presents the modulus of the probability amplitude for $\chi_1 = 0$, raised to the power $\nu = 1/4$ for the visual purpose. Panel (b) shows the phase of the amplitude modified by the phase-factor $\exp[i\phi(\mathbf{p})]$ with $\phi(\mathbf{p})$ defined by Eq. (63). Panels (c) and (d) represent the same quantities, but for $\chi_1 = \pi$.

The analysis of these distributions shows that for $\chi_1 = \pi$ the phase $\Phi_{\lambda_0}^{(\beta)}(\mathbf{p}, \lambda)$ at those lines jumps by π , which proves that the amplitude vanishes there. In contrast, for $\chi_1 = 0$ we observe isolated points for which the amplitude's phase is not defined, i.e., in their close vicinity it acquires all possible values from the range $[-\pi, \pi]$. This means that these points are the intersections of vortex lines with the (p_x, p_y) -plane. For each of these points we can determine the so-called topological charge in such a way that it is a positive integer number if during the counterclockwise rotation around this point the phase increases; otherwise, it is negative. The value of the topological charge is determined by the number of windings during such a rotation. Analysis of the presented amplitude's phase distribution shows that the topological charges of these isolated points are $+1$ (we define this point as a vortex) or -1 (anti-vortex). This means that the 'lines' of small amplitude values observed in Fig. 4(a) are in fact vortex streets, i.e. a sequence of alternating vortices and anti-vortices. Moreover, numerical analysis shows that the change of the phase χ_1 of the electric pulse leads to the change of the position of these isolated vortex points such that for $\chi_1 = \pi$ all vortices and anti-vortices are 'annihilated' and the vortex streets turn into continuous lines lying in the (p_x, p_y) -plane. Exactly the same scenario is realized in the case of ionization.

At this point, let us explain the role of the extra phase-factor $\exp[i\phi(\mathbf{p})]$, where we have assumed

$$\phi(\mathbf{p}) = 2E_p T_p = 2cT_p \sqrt{\mathbf{p}^2 + (m_e c)^2}. \quad (63)$$

This phase has been used in Eq. (62) and in the presen-

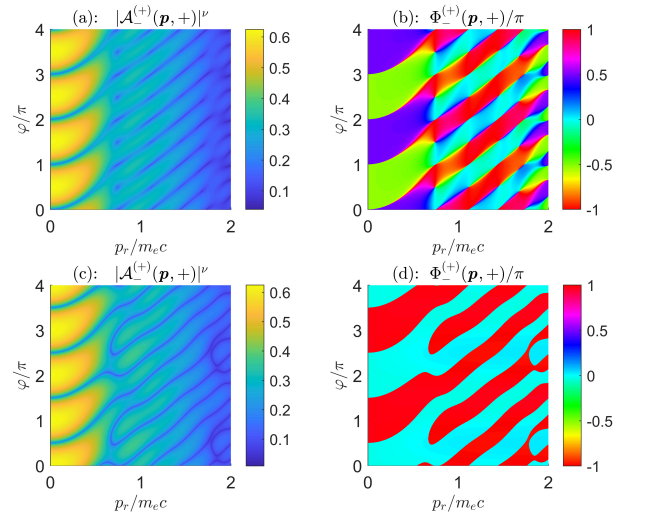


Figure 5. The same as in Fig. 4, but for the probability amplitude $\mathcal{A}^+(\mathbf{p}, +)$ and for the positron and electron helicities -1 and $+1$, respectively.

tation of the probability amplitude's phase distribution in Fig. 4. First of all, it does not modify the positions of probability amplitude zeros, but certainly alters its phase pattern. Its purpose is to reduce the rapid change of the amplitude's phase and to extract only a slowly changing part of it. In this case, its modulo 2π part is also a slowly changing function of the momentum \mathbf{p} . By doing this all singularities of complex amplitudes, i.e., the jump of the phase by π when crossing the zero-line and the winding of it around the vortex point are better visualized. Such a procedure concerning the presentation of the amplitude's phase distribution has been introduced in Ref. [29].

As mentioned above, the momentum distributions of the created pairs show a significant similarity to the momentum distributions of photoelectrons in multiphoton ionization. In the case of long electric field pulses (i.e. when $N_{\text{osc}} \gg 1$) its Fourier transform is centered around the frequency ω . Then the momentum distributions are concentrated around such energies for which $n\omega \approx 2E_p$, where n is a positive integer that can be interpreted as the number of energy quanta absorbed from the electric field during the process. The analysis for long pulses shows that in the momentum distributions maxima are observed for

$$p_r = m_e c \sqrt{\left(\frac{n\omega}{2m_e c^2}\right)^2 - 1}. \quad (64)$$

For $n = 2$ and $n = 3$ we obtain $p_r = 1.12m_e c$ and $p_r = 2.02m_e c$, respectively. Indeed, we have checked that for $N_{\text{osc}} = 30$ we observe the dominant peak for energy $E_p = \omega$. Additionally, the number of arms in the spiral distributions grows as $2n$, which is also consistent with the results obtained in multiphoton ionization.

Concluding this section, in Fig. 5 we present the distributions corresponding to the ones shown in Fig. 4, but for the opposite positron and electron helicities. Although

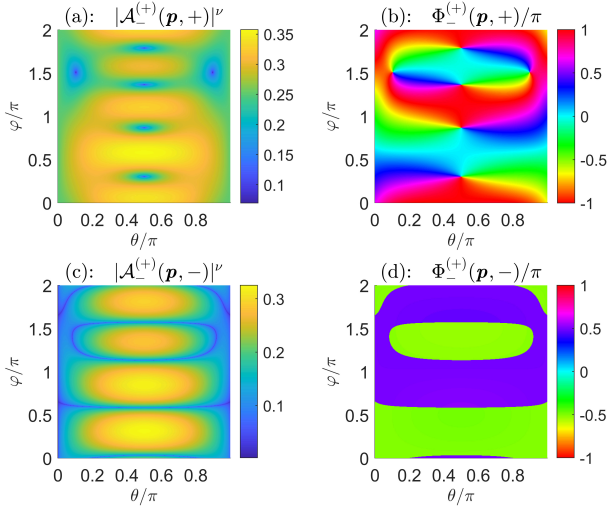


Figure 6. The same as in Figs. 4 and 5 for $\chi_1 = \pi$, but on the momentum sphere of the radius $p_r = m_e c$. These distributions show that the lines of zero probability are either parts of the nodal surfaces [Fig. 4(c)] or isolated vortex lines [Fig. 5(c)].

the patterns look very similar, their physical meaning is different. This is discussed in the next section.

B. Angular distributions for fixed energy

In Sec. IV A, it has been shown that the change of χ_1 can lead to the annihilation of quantum vortices and anti-vortices, and that the vortex street in the plane of electric field polarization transforms itself into a nodal line. The latter being the intersection of the entire nodal surface with the polarization plane. We encounter such a situation in ionization. But this is not the only possible scenario. Another possibility is that the vortex street is formed as a result of multiple passages of a wavy vortex line through a selected surface, which flattens out while changing the electric field parameters. If it additionally lies on a selected plane, it appears as a nodal line. However, it is an isolated line, as it does not belong to the nodal surface. In order to explain which scenario is realized for the helicity configurations presented in Figs. 4 and 5, we need to examine the distribution of vortices and nodal lines away from the (p_x, p_y) -plane. For instance, one can analyze momentum distributions on spheres of given momentum values, i.e., for momenta

$$\mathbf{p} = p_r (\sin \theta \cos \varphi \mathbf{e}_x + \sin \theta \sin \varphi \mathbf{e}_y + \cos \theta \mathbf{e}_z), \quad (65)$$

with fixed p_r and varied angles θ and φ .

In Fig. 6 we present the momentum distributions of the probability amplitude moduli and their phases on a sphere of radius $p_r = m_e c$ and for $\chi_1 = \pi$ for the two spin configurations discussed above. Although in the (p_x, p_y) -plane (i.e., for $\theta = \pi/2$) these distributions are very similar to each other (cf., Figs. 4 and 5 for $\chi_1 = \pi$), on the

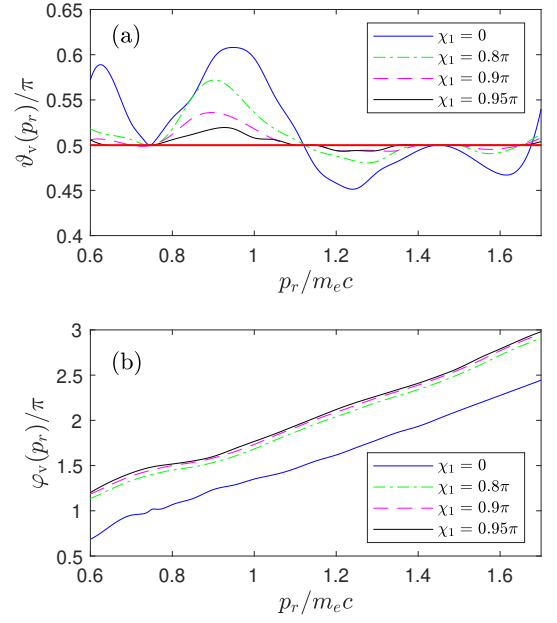


Figure 7. Transformation of a vortex line with changing the phase χ_1 . The vortex line evolves from the wavy line into the flat one lying in the plane $p_z = 0$ and presented in Fig. 5(c). In upper panel, the straight red line at $\vartheta_v(p_r)/\pi = 0.5$ corresponds to the case when $\chi_1 = \pi$. The remaining values of χ_1 are specified in the legends.

sphere they look completely different. For the spin configuration $(\lambda_0, \lambda) = (-, -)$ [cf., Figs. 4(c) and (d)] there are continuous nodal lines, indicating that these are intersections with nodal surfaces. In turn, for the spin configuration $(-, +)$ these are intersections with vortex lines lying in the $\theta = \pi/2$ plane. The nodal lines appearing for $\chi_1 = \pi$ in Fig. 5(c) are therefore vortex lines resulting from the flattening out of the wavy vortex lines observed in Fig. 5(a) as spiral vortex streets. To see this better, in Fig. 7 we present a family of trajectories of a chosen vortex line for several selected values of χ_1 and parametrized by the radial momentum p_r . The momenta defining this selected vortex line are given by the equation,

$$\mathbf{p}_v(p_r) = p_r (\sin[\vartheta_v(p_r)] \cos[\varphi_v(p_r)] \mathbf{e}_x + \sin[\vartheta_v(p_r)] \sin[\varphi_v(p_r)] \mathbf{e}_y + \cos[\vartheta_v(p_r)] \mathbf{e}_z), \quad (66)$$

with the functions $\vartheta_v(p_r)$ and $\varphi_v(p_r)$ shown in Fig. 7. As one can see, the amplitude of the oscillations of $\vartheta_v(p_r)$ in Fig. 7(a) decreases with increasing χ_1 , and for $\chi_1 = \pi$ it becomes constant and equal to $\pi/2$. Moreover, for χ_1 different from π , the vortex line is tangent to the surface $\theta = \pi/2$ at the points $(p_r, \varphi/\pi) \approx (0.75m_e c, 1)$ and $(1.45m_e c, 2)$, whereas it intersects the surface approximately at the points $(1.12m_e c, 1.5)$ and $(1.67m_e c, 2.4)$. Such behavior of the vortex line is also visible (even though it is less clear) in Fig. 5(b).

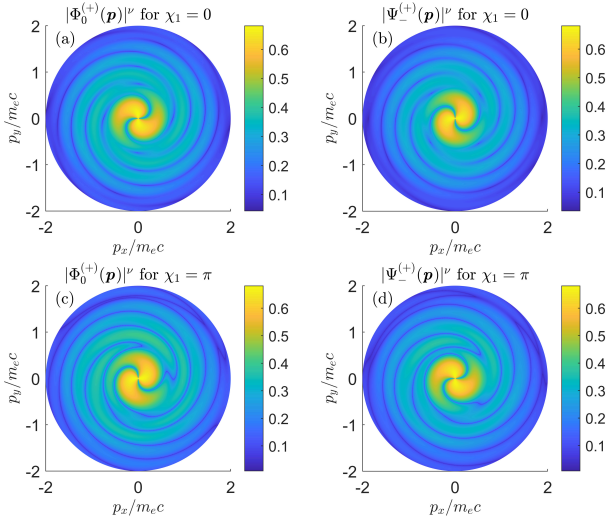


Figure 8. Probability amplitudes for the electric pulses defined in the caption to Fig. 3 for $p_z = 0$ and for the two non-vanishing helicity-entangled probability amplitudes $\Phi_0^{(+)}(\mathbf{p})$ and $\Psi_-^{(+)}(\mathbf{p})$ defined in Eq. (67). In each panel, the modulus of the probability amplitude is raised to the power $\nu = 1/4$ for the visual purpose.

V. DISTRIBUTIONS FOR HELICITY-ENTANGLED STATES

As we have already mentioned, our current approach and the scattering matrix approach [29] allow to investigate the positron and electron spin-correlation effects in the dynamical Sauter-Schwinger process. This means that, besides the problems discussed in Sec. IV, we can also study the quantum spin- or helicity-entanglement phenomenon. This expands the range of application of the DHW and QKE formalisms. Specifically, because these formalisms provide a partial information about the spin effects, as they do not account for the spin degree of freedom of the second particle (in most cases positrons) (see, e.g., [46–53]).

Following the old ideas put forward by Einstein, Podolsky and Rosen [54], Schrödinger [55, 56], and Bell [57, 58] we introduce the helicity-entangled probability amplitudes of pair creation (similar to the maximally entangled Bell states [59, 60] for two spin-1/2 systems),

$$\begin{aligned}\Phi_0^{(\beta)}(\mathbf{p}) &= \frac{1}{\sqrt{2}} [\mathcal{A}_-^{(\beta)}(\mathbf{p}, +) - \mathcal{A}_+^{(\beta)}(\mathbf{p}, -)], \\ \Psi_0^{(\beta)}(\mathbf{p}) &= \frac{1}{\sqrt{2}} [\mathcal{A}_-^{(\beta)}(\mathbf{p}, +) + \mathcal{A}_+^{(\beta)}(\mathbf{p}, -)], \\ \Psi_-^{(\beta)}(\mathbf{p}) &= \frac{1}{\sqrt{2}} [\mathcal{A}_-^{(\beta)}(\mathbf{p}, -) - \mathcal{A}_+^{(\beta)}(\mathbf{p}, +)], \\ \Psi_+^{(\beta)}(\mathbf{p}) &= \frac{1}{\sqrt{2}} [\mathcal{A}_-^{(\beta)}(\mathbf{p}, -) + \mathcal{A}_+^{(\beta)}(\mathbf{p}, +)].\end{aligned}\quad (67)$$

These formulas follow directly from the definition of an

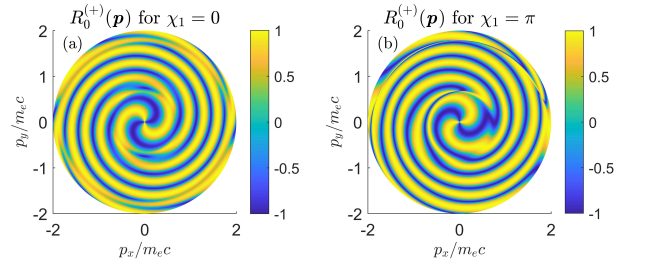


Figure 9. The asymmetry momentum distribution defined by Eq. (71) for two phases χ_1 and for the momentum distributions presented in Fig. 8.

arbitrary state of created pairs,

$$|\mathcal{A}^{(\beta)}(\mathbf{p})\rangle = \sum_{\lambda_0, \lambda = \pm} \mathcal{A}_{\lambda_0}^{(\beta)}(\mathbf{p}, \lambda) |\lambda_0\rangle \otimes |\lambda\rangle, \quad (68)$$

and the definition of the Bell states,

$$\begin{aligned}|\Phi_0\rangle &= \frac{1}{\sqrt{2}} (|-\rangle \otimes |+\rangle - |+\rangle \otimes |-\rangle), \\ |\Psi_0\rangle &= \frac{1}{\sqrt{2}} (|-\rangle \otimes |+\rangle + |+\rangle \otimes |-\rangle), \\ |\Psi_-\rangle &= \frac{1}{\sqrt{2}} (|-\rangle \otimes |-\rangle - |+\rangle \otimes |+\rangle), \\ |\Psi_+\rangle &= \frac{1}{\sqrt{2}} (|-\rangle \otimes |-\rangle + |+\rangle \otimes |+\rangle),\end{aligned}\quad (69)$$

where $|\lambda_0\rangle \otimes |\lambda\rangle$ means the helicity product state of created particles. In the following, we shall refer to $|\Phi_0\rangle$ as a singlet state, whereas to the remaining states as a triplet of states. Note that

$$\Phi_0^{(\beta)}(\mathbf{p}) = \langle \Phi_0 | \mathcal{A}^{(\beta)}(\mathbf{p}) \rangle, \quad (70)$$

and similarly for the remaining probability amplitudes.

Fig. 8 shows the distributions of the amplitude moduli, $|\Phi_0^{(+)}(\mathbf{p})|$ and $|\Psi_-^{(+)}(\mathbf{p})|$, for the two carrier-envelope phases of the electric pulse discussed above, $\chi_1 = 0$ and π . The remaining distributions defined by Eq. (67) vanish for $p_z = 0$. Similarly to the cases discussed in Sec. IV A, the vortex structures appear explicitly for $\chi_1 = 0$. However, for $\chi_1 = \pi$ they disappear for the $\Phi_0^{(+)}(\mathbf{p})$ distribution (i.e., are transformed into nodal lines, which are part of the nodal surfaces intersecting the $p_z = 0$ plane), while for the $\Psi_-^{(+)}(\mathbf{p})$ distribution they evolve with the changing χ_1 into isolated vortex lines in the $p_z = 0$ plane. The phase distributions of these amplitudes look similar to the ones discussed above and therefore the corresponding figures are not presented.

To investigate the correlations between the generation of pairs in the Bell states $|\Phi_0\rangle$ and $|\Psi_-\rangle$, we introduce the asymmetry momentum distribution,

$$R_0^{(\beta)}(\mathbf{p}) = \frac{|\Phi_0^{(\beta)}(\mathbf{p})|^2 - |\Psi_-^{(\beta)}(\mathbf{p})|^2}{|\Phi_0^{(\beta)}(\mathbf{p})|^2 + |\Psi_-^{(\beta)}(\mathbf{p})|^2}. \quad (71)$$

This distribution determines for which momenta \mathbf{p} the pair is created in one of these entangled helicity states. That is, if for a chosen momentum $R_0^{(\beta)}(\mathbf{p})$ is close to 1 or -1 , then the pair appears in the Bell state $|\Phi_0\rangle$ or $|\Psi_-\rangle$, respectively. The asymmetry distributions for two chosen electric field phases, $\chi_1 = 0$ and $\chi_1 = \pi$, are presented in Fig. 9. We can see that although they have similar spiral structures, they are however rotated with respect to each other by approximately $\pi/2$ (at least for momenta $p_r < m_e c/2$). This means that if for a chosen momenta \mathbf{p} for the phase $\chi_1 = 0$ the pair is generated in the state $|\Phi_0\rangle$, then for the phase $\chi_1 = \pi$ it can be created in state $|\Psi_-\rangle$. Thus, the applied electric field can be used not only for controlling the generation of selected entangled states, but also can act as a switch between them. This seems to be interesting for the rapidly developing area of strong-field quantum simulations, as discussed for instance in [30] mainly for the Breit-Wheeler process.

As mentioned above, in the plane $p_z = 0$ (and at least for the electric field pulse considered in this paper), pairs are created only in two entangled states. In general, however, all states are realized in this process. To take into account such a situation, let us introduce an asymmetry distribution that discriminates only between the singlet state $|\Phi_0\rangle$ and three remaining states,

$$R^{(\beta)}(\mathbf{p}) = \frac{|\Phi_0^{(\beta)}(\mathbf{p})|^2 - P_{\Psi}^{(\beta)}(\mathbf{p})}{|\Phi_0^{(\beta)}(\mathbf{p})|^2 + P_{\Psi}^{(\beta)}(\mathbf{p})}, \quad (72)$$

where

$$P_{\Psi}^{(\beta)}(\mathbf{p}) = |\Psi_0^{(\beta)}(\mathbf{p})|^2 + |\Psi_-^{(\beta)}(\mathbf{p})|^2 + |\Psi_+^{(\beta)}(\mathbf{p})|^2. \quad (73)$$

The corresponding distributions are presented in Fig. 10. As we see, for $p_r = m_e c/2$ the change of the phase χ_1 from 0 to π can serve as the switch between the singlet and triplet entangled states. For larger p_r this goal can not be achieved for the electric field parameters considered here. However, we have checked that by changing the phase χ_1 from 0 to $\pi/2$ the similar switching is available also for $p_r = m_e c$.

In summary, we note that the asymmetry distributions do not depend on the way how the initial state is normalized (as mentioned earlier, this is an important feature that distinguishes relativistic quantum field theory from condensed matter physics). This means that the analysis presented here can be applied to similar problems studied in condensed matter physics, where the equivalent of electron-positron pair production is the excitation of an electron to the conduction band and the creation of a hole in the valence band. The unquestionable advantage of such studies is that in this case the electric field intensities necessary to observe the above-mentioned effect are experimentally achievable. Therefore, the analysis presented here fits into the general trend observed in condensed matter physics, which does not consist in modifying the material medium itself, forcing a change of the band structure in the desired manner, but rather in applying an external electromagnetic field (usually laser

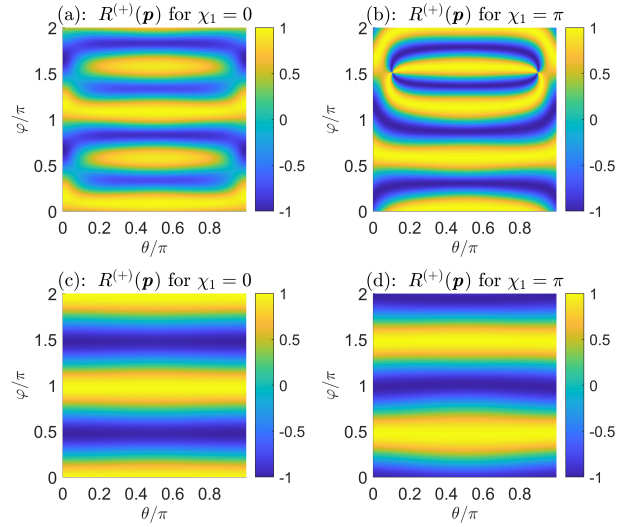


Figure 10. The asymmetry momentum distribution defined by (72) for two phases χ_1 and for the momentum distributions calculated on the sphere of momenta (65) for $p_r = m_e c$ [panels (a) and (b)], and $p_r = m_e c/2$ [panels (c) and (d)].

pulses), which dynamically changes the band structure on a very short time scale. The recently popular Floquet engineering is an example of such investigations [61–70]. Regardless of the above, the study of strong-field QED remains important from the fundamental point of view.

VI. CONCLUSIONS

The Dirac two photon pair annihilation process and the Breit-Wheeler two photon pair creation process inspired Heisenberg and Euler, and later Schwinger, to consider the concept of the effective Lagrangian of QED and to investigate the pair creation by a constant electromagnetic fields (see, e.g., [13] for historical notes). Direct experimental verification of this phenomenon, however, requires very strong fields, which are unattainable experimentally. For this reason, research has recently been conducted on the dynamical Sauter-Schwinger effect with the hope that in the near future pulsed electric fields of intensities close to the Schwinger limit will be generated in the laboratory, resulting for instance from the concentration of many laser pulses in a small volume and in a short time. Regardless of this, the equivalent processes to the Sauter-Schwinger effect are already realized in condensed matter physics or photonics. Therefore, studying this phenomenon in its 'purest' form, i.e., in relativistic QED, is purposeful, because in this way new approaches or concepts are developed. In this respect, the situation encountered in the case of the Sauter-Schwinger effect is not unique, as there are many other examples of theoretical research that for many years were not experimentally confirmed (e.g., gravitational waves [71] or Bose-Einstein condensates [72]). We also meet a similar situation in

the case of certain theoretical concepts (e.g., Majorana fermions [73]), which are being revived in other areas of physics.

The aim of this paper was to investigate helicity correlations and entanglement in the electron-positron pair creation by a time-dependent pulsed electric field. Also, we have analyzed topological effects appearing in the momentum distributions of created particles. To achieve these goals, we have used the approach which is equivalent to the scattering matrix formalism [29], but is more straightforward. Namely, we have demonstrated that the Sauter-Schwinger process can be fully described by the Dirac equation [28] (i.e., without the need for the second quantization formalism) with appropriately chosen boundary conditions. We have shown that, for the considered electric field pulses, vortex structures in the momentum distributions of created particles significantly depend on helicity correlations. This is in contrast to spiral structures, which are only slightly modified by changing the helicities of the particles. These conclusions are also valid when the applied electric field changes. Additionally, we have investigated the generation of helicity-

entangled states and have demonstrated that the electric field can play the role of a switch between different entangled states. We suppose that this result can be applied in quantum simulations within strong-field QED for various scenarios of the electron-positron pair creation, for instance, for the Breit-Wheeler process [30, 32] or the trident one [31]. We also assume that these results can be used in the analysis of processes occurring in condensed matter physics. Finally, we would like to note that for the considered laser field such that $|\mathcal{E}(t)| \ll \mathcal{E}_S$, the momentum distributions presented in this work after summing them up over the helicity (spin) degrees of freedom are nearly identical to the respective distributions calculated with the DHW or the QKE formalisms.

ACKNOWLEDGEMENTS

We would like to thank E. Saczuk and F. Cajiao Vélez for discussions.

-
- [1] P. A. M. Dirac, Proc. R. Soc. London. Ser. A, **117**, 610 (1928).
 - [2] S. Tomonaga, Prog. Theor. Phys. **1**, 27 (1946).
 - [3] R. P. Feynman, Phys. Rev. **76**, 749 (1949).
 - [4] R. P. Feynman, Phys. Rev. **76**, 769 (1949).
 - [5] J. Schwinger, Phys. Rev. **82**, 664 (1951).
 - [6] F. J. Dyson, Phys. Rev. **75**, 486 (1949).
 - [7] F. J. Dyson, Phys. Rev. **75**, 1736 (1949).
 - [8] J. Schwinger (ed), *Quantum Electrodynamics* (Dover, New York, 1958).
 - [9] W. Heisenberg and H. Euler, Zeit. Phys. **98**, 714 (1936).
 - [10] F. Sauter, Zeit. Phys. **69**, 742 (1931).
 - [11] S. S. Schweber, *An Introduction to Relativistic Quantum Field Theory* (Harper and Row, New York, 1961).
 - [12] S. S. Schweber, Rev. Mod. Phys. **58**, 449 (1986).
 - [13] R. Ruffini, G. Vereshchagin, and S.-S. Xue, Phys. Rep. **487**, 1 (2010).
 - [14] F. Cajiao Vélez, J. Z. Kamiński, and K. Krajewska, Atoms **7**, 34 (2019).
 - [15] I. Białynicki-Birula, P. Górnicki, and J. Rafelski, Phys. Rev. D **44**, 1825 (1991).
 - [16] I. Białynicki-Birula, M. Cieplak, and J. Kamiński, *Theory of Quanta* (Oxford, New York, 1992).
 - [17] F. Hebenstreit, R. Kämpfer, and H. Gies, Phys. Rev. D **82**, 105026 (2010).
 - [18] C. Kohlfürst, Phys. Rev. D **101**, 096003 (2020).
 - [19] A. Otto, D. Seipt, D. Blaschke, S. A. Smolyansky, and B. Kämpfer, Phys. Rev. D **91**, 105018 (2015).
 - [20] J. Z. Kamiński, M. Twardy, and K. Krajewska, Phys. Rev. D **98**, 056009 (2018).
 - [21] D. B. Blaschke, B. Kämpfer, S. M. Schmidt, A. D. Panferov, A. V. Prozorkevich, and S. A. Smolyansky, Phys. Rev. D **88**, 045017 (2013).
 - [22] C. K. Dumlu, Phys. Rev. D **79**, 065027 (2009).
 - [23] K. Krajewska and J. Z. Kamiński, Phys. Rev. A **100**, 012104 (2019).
 - [24] H. Al-Naseri, J. Zamanian, and G. Brodin, Phys. Rev. E **104**, 015207 (2021).
 - [25] A. Blinne and H. Gies, Phys. Rev. D **89**, 085001 (2014).
 - [26] A. Blinne and E. Strobels, Phys. Rev. D **93**, 025014 (2016).
 - [27] T. Cheng, Q. Su, and R. Grobe, Contemp. Phys. **51**, 315 (2010).
 - [28] A. Bechler, F. C. Vélez, K. Krajewska, and J. Z. Kamiński, Acta Phys. Pol. A **143**, S18 (2023), <https://doi.org/10.48550/arXiv.2306.07668>.
 - [29] M. M. Majczak, K. Krajewska, J. Z. Kamiński, and A. Bechler, Phys. Rev. D **110**, 116025 (2024), <https://doi.org/10.48550/arXiv.2403.15206>.
 - [30] L. Hidalgo and P. Draper, Phys. Rev. D **109**, 076004 (2024).
 - [31] S. P. Roshchupkin and M. V. Shakhov, Photonics **12**, 307 (2025).
 - [32] S. Tang, B. M. Dillon, and B. King, arXiv:hep-ph/2504.06338v1 (2025).
 - [33] J. Z. Kamiński and E. Saczuk, Phys. Lett. A **375**, 251 (2011).
 - [34] J. Z. Kamiński, E. Saczuk, and F. Cajiao Vélez, Ann. Phys. (Berlin) **525**, 118 (2013).
 - [35] I. Białynicki-Birula and Z. Białynicka-Birula, *Quantum Electrodynamics* (Pergamon, Oxford, 1975).
 - [36] J. M. Ngoko Djiokep, S. X. Hu, L. B. Madsen, N. L. Manakov, A. V. Meremianin, and A. F. Starace, Phys. Rev. Lett. **115**, 113004 (2015).
 - [37] P. A. M. Dirac, Proc. R. Soc. London, Ser. A **133**, 60 (1931).
 - [38] I. Białynicki-Birula, Z. Białynicka-Birula, and C. Śliwa, Phys. Rev. A **61**, 032110 (2000).

- [39] M. C. Suster, J. Derlikiewicz, J. Z. Kamiński, and K. Krajewska, *Opt. Express* **32**, 6085 (2024).
- [40] M. A. H. B. Md Yusoff, J. M. Ngoko Djiokap, A. V. Meremianin, and N. L. Manakov, *Phys. Rev. A* **110**, 023102 (2024).
- [41] L. Geng, F. Cajiao Vélez, J. Z. Kamiński, L.-Y. Peng, and K. Krajewska, *Phys. Rev. A* **102**, 043117 (2020).
- [42] N. V. Larionov, S. Y. Ovchinnikov, A. A. Smirnovsky, and A. A. Schmidt, *Tech. Phys.* **63**, 1569 (2018).
- [43] F. Cajiao Vélez, L. Geng, J. Z. Kamiński, L.-Y. Peng, and K. Krajewska, *Phys. Rev. A* **102**, 043102 (2020).
- [44] L. Geng, F. Cajiao Vélez, J. Z. Kamiński, L.-Y. Peng, and K. Krajewska, *Phys. Rev. A* **104**, 033111 (2021).
- [45] M. M. Majczak, F. C. Vélez, J. Z. Kamiński, and K. Krajewska, *Opt. Express* **30**, 43330 (2022).
- [46] L.-N. Hu, H.-H. Fan, O. Amat, S. Tang, and B.-S. Xie, *Phys. Rev. D* **110**, 056013 (2024).
- [47] O. Amat, H.-H. Fan, S. Tang, Y.-F. Huang, and B.-S. Xie, *Phys. Rev. D* **111**, 056020 (2025).
- [48] C. Kohlfürst, *Phys. Rev. D* **99**, 096017 (2019).
- [49] X.-G. Huang and H. Taya, *Phys. Rev. D* **100**, 016013 (2019).
- [50] Z. L. Li, Y. J. Li, and B. S. Xie, *Phys. Rev. D* **96**, 076010 (2017).
- [51] L.-N. Hu, O. Amat, L. Wang, A. Sawut, H.-H. Fan, and B. S. Xie, *Phys. Rev. D* **107**, 116010 (2023).
- [52] I. A. Aleksandrov, A. Kudlis, and A. I. Klochai, *Phys. Rev. Res.* **6**, 043009 (2024).
- [53] I. A. Aleksandrov and A. Kudlis, *Phys. Rev. D* **110**, L011901 (2024).
- [54] A. Einstein, B. Podolsky, and N. Rosen, *Phys. Rev.* **47**, 777 (1935).
- [55] E. Schrödinger, *Naturwiss.* **23**, 807 (1935).
- [56] E. Schrödinger, *Math. Proc. Cambridge Phil. Soc.* **31**, 555 (1935).
- [57] J. S. Bell, *Physics Physique Fizika* **1**, 195 (1964).
- [58] J. S. Bell, *Rev. Mod. Phys.* **38**, 447 (1966).
- [59] N. D. Mermin, *Quantum Computer Science* (Cambridge, New York, 2007).
- [60] M. Le Bellac, *A Short Introduction to Quantum Information and Quantum Computation* (Cambridge, New York, 2006).
- [61] K. Uchida, S. Kusaba, K. Nagai, T. N. Ikeda, and K. Tanaka, *Science Advances* **8**, eabq7281 (2022).
- [62] M. Borsch, M. Meierhofer, R. Huber, and M. Kira, *Nature Reviews Materials* **8**, 668 (2023).
- [63] V. Tiwari, B. Gu, and I. Franco, *Phys. Rev. B* **108**, 064308 (2023).
- [64] Y. Kim and J. Lee, *Materials Today Physics* **21**, 100525 (2021).
- [65] D. Popova-Gorelova and R. Santra, *Structural Dynamics* **11**, 014102 (2024).
- [66] Y. Bai, N. Li, R. Li, and P. Liu, *Advances in Physics: X* **7**, 2013134 (2022).
- [67] B. Dey and T. K. Ghosh, *Phys. Rev. B* **98**, 075422 (2018).
- [68] F. H. M. Faisal and J. Z. Kamiński, *Phys. Rev. A* **56**, 748 (1997).
- [69] P.-H. Fu, S. Mondal, J.-F. Liu, Y. Tanaka, and J. Cayao, *arXiv:cond-mat.supr-con/2505.20205* (2025).
- [70] T. Oka and S. Kitamura, *Ann. Rev. Cond. Mat. Phys.* **10**, 387 (2019).
- [71] N. Christensen and R. Meyer, *Rev. Mod. Phys.* **94**, 025001 (2022).
- [72] F. Dalfovo, S. Giorgini, L. P. Pitaevskii, and S. Stringari, *Rev. Mod. Phys.* **71**, 463 (1999).
- [73] Y. Tanaka, S. Tamura, and J. Cayao, *Prog. Theor. Exp. Phys.* **2024**, 08C105 (2024).